All-optical wavelength conversion based on time-domain holography

María R. Fernández-Ruiz,[1,*] Lei Lei,[1] Martin Rochette,[2] and José Azaña[1]

[1]*Institut National de la Recherche Scientifique – Énergie, Matériaux et Télécommunications (INRS- EMT), Montréal, QC, H5A 1K6, Canada*

[2]*Department of Electrical and Computer Engineering, McGill University, Montréal, QC, H3A 2A7, Canada*

[*]*ruiz@emt.inrs.ca*

Abstract: All-optical wavelength conversion of a complex (amplitude and phase) optical signal is proposed based on an all-optical implementation of time-domain holography. The temporal holograms are generated through a cross-phase modulation (XPM) process in a highly-nonlinear optical fiber, avoiding the necessity of accomplish the phase matching condition between the involved pump and probe signals, and reducing the power requirements compared to those of the traditional wavelength conversion implementations using four wave mixing (FWM). The proposed scheme also achieves symmetric conversion efficiency for up- and down-conversion. As a proof-of-concept, wavelength conversion of a train of 10 GHz chirped Gaussian-like pulses and their conjugated is experimentally demonstrated.

OCIS codes: (190.0190) Nonlinear optics; (320.0320) Ultrafast optics; (090.0090) Holography; (030.1670) Coherent optical effects; (230.7405) Wavelength conversion devices.

References and links

1. K. Kikuchi, "Coherent Optical Communications: Historical Perspectives and Future Directions," in M. Nakazawa, K. Kikuchi and T. Miyazaki. (eds.) *High spectral density optical communication technologies*, Optical and Fiber Communications reports **6**, (Springer-Verlag Berlin Heidelberg, 2010).
2. S. L. Danielsen, P. B. Hansen, and K. E. Stubkjaer, "Wavelength conversion in optical packet switching," J. Lightwave Technol. **16**(12), 2095–2108 (1998).
3. R. Adams, M. Spasojevic, M. Chagnon, M. Malekiha, J. Li, D. V. Plant, and L. R. Chen, "Wavelength conversion of 28 Gbaud 16-QAM signals based on four-wave mixing in a silicon nanowire," Opt. Express **22**(4), 4083–4090 (2014).
4. G. W. Lu, T. Sakamoto, and T. Kawanishi, "Wavelength conversion of optical 64QAM through FWM in HNLF and its performance optimization by constellation monitoring," Opt. Express **22**(1), 15–22 (2014).
5. A. D'Ottavi, P. Spano, G. Hunziker, R. Paiella, R. Dall'Ara, G. Guekos, and K. J. Vahala, "Wavelength conversion at 10 Gb/s by four-wave mixing over a 30-nm interval," IEEE Photonics Technol. Lett. **10**(7), 952–954 (1998).
6. L. Xu, N. Ophir, M. Menard, R. K. W. Lau, A. C. Turner-Foster, M. A. Foster, M. Lipson, A. L. Gaeta, and K. Bergman, "Simultaneous wavelength conversion of ASK and DPSK signals based on four-wave-mixing in dispersion engineered silicon waveguides," Opt. Express **19**(13), 12172–12179 (2011).
7. J. Ma, J. Yu, C. Yu, Z. Jia, X. Sang, Z. Zhou, T. Wang, and G. K. Chang, "Wavelength conversion based on four-wave mixing in high-nonlinear dispersion shifted fiber using a dual-pump configuration," J. Lightwave Technol. **24**(7), 2851–2858 (2006).
8. M. F. Huang, J. Yu, and G. K. Chang, "Polarization insensitive wavelength conversion for 4x112Gbit/s polarization multiplexing RZ-QPSK signals," Opt. Express **16**(26), 21161–21169 (2008).
9. J. Yu, X. Zheng, C. Peucheret, A. T. Clausen, H. N. Poulsen, and P. Jeppesen, "40-Gb/s all-optical wavelength conversion based on a nonlinear optical loop mirror," J. Lightwave Technol. **18**(7), 1001–1006 (2000).
10. M. Galili, L. K. Oxenløwe, H. C. H. Mulvad, A. T. Clausen, and P. Jeppesen, "Optical wavelength conversion by cross-phase modulation of data signals up to 640 Gb/s," IEEE J. Sel. Top. Quantum Electron. **14**(3), 573–579 (2008).
11. B. E. Olsson, P. Ohlen, L. Rau, and D. J. Blumenthal, "A simple and robust 40-Gb/s wavelength converter using fiber cross-phase modulation and optical filtering," IEEE Photonics Technol. Lett. **12**(7), 846–848 (2000).
12. C. H. Kwok, S. H. Lee, K. K. Chow, C. Shu, C. Lin, and A. Bjarklev, "Widely tunable wavelength conversion with extinction ratio enhancement using PCF-based NOLM," IEEE Photonics Technol. Lett. **17**(12), 2655–2657 (2005).

#242996 Received 15 Jun 2015; revised 14 Aug 2015; accepted 16 Aug 2015; published 21 Aug 2015

13. G. P. Agrawal, *Nonlinear Fiber Optics*, 3rd ed. (Academic, 2001).
14. S. Ayotte, H. Rong, S. Xu, O. Cohen, and M. J. Paniccia, "Multichannel dispersion compensation using a silicon waveguide-based optical phase conjugator," Opt. Lett. **32**(16), 2393–2395 (2007).
15. M. R. Fernández-Ruiz, M. Li, and J. Azaña, "Time-domain holograms for generation and processing of temporal complex information by intensity-only modulation processes," Opt. Express **21**(8), 10314–10323 (2013).
16. A. V. Oppenheim and A. S. Willsky, *Signals and Systems*, 2nd ed. (Prentice-Hall, 1996).
17. Y. Chen, "Four-wave mixing in optical fibers: exact solution," J. Opt. Soc. Am. B **6**(11), 1986–1993 (1989).

1. Introduction

Wavelength division multiplexing (WDM) systems have allowed a rapid increase in the spectral efficiency of optical networks in the last decades, through the multiplexing of multiple optical channels into a single optical fiber by using different wavelengths [1]. All-optical wavelength conversion is a fundamental process in high-speed WDM systems, ensuring full flexibility in the network, preventing wavelength blocking, and allowing high-speed operation while avoiding inefficient electro-optics conversion [2–12]. Recently, there has been a renewed interest in coherent technologies [1,3,4], with the aim of a further increase in the spectral efficiency of the optical telecommunications systems by means of the use of high order modulation formats. Thus, wavelength conversion of complex (amplitude and phase) information signals is especially desired.

A number of all-optical wavelength conversion techniques have appeared in the last few decades. Most of them rely on parametric nonlinear effects, such as four-wave mixing (FWM) [2–8]. However, FWM-based schemes present several drawbacks that limit their practical application, which include (i) the need to satisfy a stringent phase-matching condition, which either limits the wavelength conversion tunability or requires using dispersion-engineered media [3,6,13]; (ii) the need to use very high power for the involved signals (typically, >10dBm average powers) and (iii) the fact that the wavelength converted signal is phase conjugated in time with respect to the original one when using the higher efficiency configurations, e.g. one [3–6] or two [7,8] continuous wave (CW) pumps (in general, phase conjugation depends on the configuration of the pumps and signal). Whereas all-optical temporal conjugation of data signals is also desired for a range of operations in fiber-optics communication links [14], in order to achieve wavelength conversion of the original signal, a second conjugation process, typically another FWM stage, is required. Alternatively, wavelength conversion schemes have been proposed based on cross-phase modulation (XPM). XPM is, in general, easier to excite than FWM since it is not conditioned to a phase matching between the probe and the pump. In these schemes, wavelength conversion is achieved from the intensity modulation of a probe CW light with a high power pump signal (the information signal) through a stage of XPM into an interferometric configuration, e.g., such as a Sagnac interferometer [9,10]; or through the sideband filtering of the output [11,12]. However, these configurations are limited to wavelength conversion of amplitude-only data signals.

In this paper, we propose and experimentally demonstrate a novel scheme for wavelength conversion of complex (amplitude and phase) optical signals using an all-optical implementation of the concept of time-domain holography [15]. Time-domain holography has been recently proposed as a method to achieve both amplitude and phase modulation of a time-domain optical signal by means of an intensity-only modulation process and a band-pass filter [15]. Wavelength conversion is considered as a modulation process where the complex envelope of the information signal modulates a different carrier signal. In the presented scheme, the temporal holograms are generated by phase-only modulation, namely XPM, in a highly-nonlinear fiber (HNLF). The scheme inherently provides a wavelength-converted temporal conjugated copy of the original signal additional to the non-conjugated copy. Although the proposed configuration is similar to that of FWM-based schemes [7,8], it avoids the need to satisfy the phase matching condition and also relaxes significantly the power requirements. In our experimental tests, we achieve down and up conversion of a train of

#242996 Received 15 Jun 2015; revised 14 Aug 2015; accepted 16 Aug 2015; published 21 Aug 2015

chirped Gaussian-like pulses with a similar efficiency (~−20 dB [3–8]) but using much lower power levels than previous FWM-based configurations (e.g., ~0.4 dBm and ~3 dBm signal and probe powers, respectively).

2. Theoretical analysis

The physical mechanism to achieve wavelength conversion of a complex optical signal involves generating an optical temporal hologram [15] through linear interference between the optical input signal to be processed, $e_S(t)$ and a coherent CW light beam, that we call *reading signal*, $e_{LO,1}(t)$. An optical coupler (OC) performs the operation of interference. Following the terminology of classical holography, the temporal hologram is the intensity of the interference signal, which contains information of the amplitude and phase of $e_S(t)$. This temporal hologram, $P_{pump}(t)$, is expressed as,

$$P_{pump}(t) \propto \left|e_S(t) + je_{LO,1}(t)\right|^2 = i_{LO,1} + \left|e_S(t)\right|^2 + 2\sqrt{i_{LO,1}}\left|e_{s0}(t)\right|\sin\left(2\pi f_i t + \angle e_{s0}(t) - \angle e_{LO,1}(t)\right), \quad (1)$$

where $j = \sqrt{-1}$, representing the π/2 phase difference induced by the OC, the information signal is defined as $e_S(t) = e_{s0}(t)\cdot\exp\{j2\pi f_S t\}$, with f_S being the signal's original carrier frequency, and $e_{s0}(t) = |e_{s0}(t)|\exp\{j\angle e_{s0}(t)\}$ being its complex envelope; the reading signal is centered at $f_{LO,1}$, $e_{LO,1}(t) = \sqrt{i_{LO,1}}\cdot\exp\{j2\pi f_{LO,1}t + \angle e_{LO,1}(t)\}$; and f_i is an intermediate frequency, $f_i = f_S - f_{LO,1}$. As $e_{LO,1}(t)$ is a coherent CW signal, its phase $\angle e_{LO,1}(t)$ can be omitted for simplicity. In general, the signals $e_{LO,1}(t)$ and $e_S(t)$ do not need to be locked for the proper operation of the method. $P_{pump}(t)$ acts as the pump in the following XPM stage.

According to holography's theory, amplitude modulation of a reference signal is required to generate the desired complex signal from the information encoded in the hologram. However, under certain conditions, phase modulation can also be applicable, as we detail in what follows. The reference signal is a low-power CW light beam, the *writing signal* $e_{LO,2}(t) = \sqrt{i_{LO,2}}\cdot\exp\{j2\pi f_{LO,2}t\}$ with carrier frequency $f_{LO,2}$. Both the pump and reference signals then propagate through a HNLF, and the expression of the reference after undergoing XPM is

$$e_{out}(t) = e_{LO,2}(t)\exp\left\{j2\gamma P_{pump}(t)L\right\}, \quad (2)$$

where γ and L are the nonlinear coefficient and the length of the HNLF, respectively. Substituting Eq. (1) into Eq. (2), we observe that the first term of $P_{pump}(t)$ just adds a constant phase to $e_{out}(t)$, so it will not be considering in the following analysis. In addition, the second term ($|e_S(t)|^2$) can be neglected if $i_{LO,1} >> |e_S(t)|^2$. This last condition is generally employed in holographic configurations to increase spectral efficiency since it relaxes the bandwidth constraints of $e_{out}(t)$ from $\geq 4B$ to $\geq 2B$ [15], in which B is the full frequency bandwidth of $e_S(t)$. The resulting expression for $e_{out}(t)$ is then

$$e_{out}(t) \approx e_{LO,2}(t)\exp\left\{j2\gamma L\sqrt{i_{LO,1}}\left|e_{s0}(t)\right|\sin\left(2\pi f_i t + \angle e_{s0}(t)\right)\right\}. \quad (3)$$

If $2\gamma L\sqrt{i_{LO,1}}\left|e_{s0}(t)\right| << \pi$, Eq. (3) can be further simplified to

#242996 Received 15 Jun 2015; revised 14 Aug 2015; accepted 16 Aug 2015; published 21 Aug 2015

$$e_{out}(t)=\sqrt{i_{LO,2}}\exp\{2\pi f_{LO,2}t\}\left(1+j2\gamma L\sqrt{i_{LO,1}}\left|e_{s0}(t)\right|\sin\left(2\pi f_i t+\angle e_{s0}(t)\right)\right). \quad (4)$$

Equation (4) shows that $e_{out}(t)$ has three components in the spectral domain: (i) a pure tone at $f_{LO,2}$, (ii) a copy of $e_S(t)$ centered at $f_{out,S}=f_{LO,2}+f_i$, and (iii) a copy of the temporal conjugate of $e_S(t)$ ($e_S^*(t)$) centered at $f_{out,-S}=f_{LO,2}-f_i$ (Fig. 1). These components are well separated in the spectral domain if $f_i \geq 2B$. Finally, a bandpass optical filter (BPF) is required to select either the wavelength converted signal (@ $f_{out,S}$) or its temporal conjugate (@ $f_{out,-S}$).

Figure 1(b) illustrates the spectra at the input of the HNLF and at its output, where a component proportional to $e_S(t)$ and to its conjugate have been generated around $e_{LO,2}(t)$ through XPM. An additional copy of $e_S^*(t)$ (depicted in grey in Fig. 1(b.2)) is expected to be induced around $e_{LO,1}(t)$ by degenerate FWM between this CW pump and the input signal.

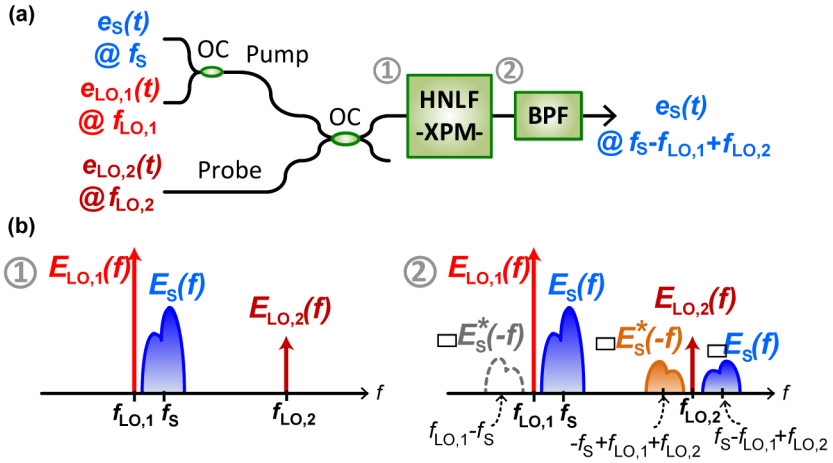

Fig. 1. (a) Scheme for performing wavelength conversion based on XPM; (b) Spectra before and after the high nonlinear fiber (HNLF): Blue components represent the information signal, the yellow component represents the conjugated signal and the dashed grey component represents the conjugated signal resulting from FWM between the pump's components.

Take note that an exact copy of $e_S(t)$ and $e_S^*(t)$ appears at the frequencies $f_{out,S}$ and $f_{out,-S}$ only if the condition $2\gamma L\sqrt{i_{LO,1}}\left|e_{s0}(t)\right| \ll \pi$ is fulfilled. In this case, the phase modulation is within the regime of *narrowband phase modulation* [16] and it affects the writing signal $e_{LO,2}(t)$ in the same manner as an intensity modulation process, causing a spectral broadening around $f_{LO,2}$ proportional to $P_{Pump}(t)$. In this case, the occurrence of FWM in the HNLF (in case the required conditions are satisfied, e.g., phase matching condition) can add up power at the spectral regions of interest, i.e., an idler component proportional to $e_S(t)$ and $e_S^*(t)$ will appear at the frequencies $f_{out,S}$ and $f_{out,-S}$, respectively, which add coherently with the results of the XPM process.

3. Simulation results

In this section, we present two numerical simulations to validate the proposed scheme. In the first example, a HNLF with dispersion curve that ensures that phase matching condition is not

#242996 Received 15 Jun 2015; revised 14 Aug 2015; accepted 16 Aug 2015; published 21 Aug 2015

satisfied is used. Thus, this example illustrates the capability of XPM-only for realizing the complex wavelength conversion process. In the second example, the parameters of the HNLF available in our laboratory are employed. In both cases, the input signal $e_S(t)$ is a train of 2 ps-FWHM Gaussian-like pulses with a repetition rate of 10 GHz, dispersed by a 1-km single-mode fiber (SMF) section. The dispersed pulses are centered at f_S = 193.79 THz ($\lambda_S = c/f_S$ = 1547 nm, with c being the speed of light.) and have an average power of 0.4 dBm. The FWHM of the pulses after the dispersion is 30 ps and the full bandwidth (at 1% of the maximum amplitude) of $e_S(t)$ is B ~800 GHz (6 nm). The reading signal $e_{LO,1}(t)$ has a central frequency of $f_{LO,1}$ = 193.41 THz ($\lambda_{LO,1}$ = 1550 nm) and an average power of 13 dBm, while the writing signal $e_{LO,2}(t)$ is centered at $f_{LO,2}$ = 195.57 THz ($\lambda_{LO,2}$ = 1533 nm) and has an average power of only 3 dBm. All these parameters well accomplish the conditions established in Section 2. Based on these settings, the wavelength converted signal is expected at $\lambda_{out,S}$ = 1530 nm.

The specifications for the HNLF in the first example are γ = 11.3 $W^{-1}km^{-1}$, L = 1015 m, the zero dispersion wavelength (ZDW) is 1540 nm and the dispersion slope S_0 (at 1540 nm) = 0.092 $ps/nm^2/km$. To check if the phase matching condition is accomplished in this case, we first derive the equations for the phase mismatch. The spectral locations of the different involved signals are illustrated in Fig. 2, where we define the parameters $\Delta\omega_p$ and $\Delta\omega_s$ to be employed in the derivation of the phase mismatch.

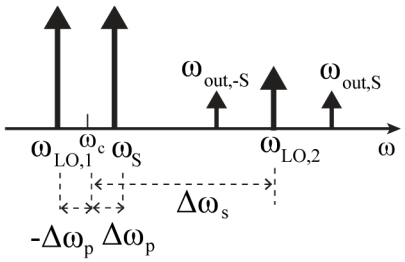

Fig. 2. Scheme of the central frequency of the signals involved in the wavelength conversion process and nomenclature given to the spectral separation between signals to develop the equations of phase-matching condition (see Eq. (5)).

Thus, the effective phase mismatch of the resulting wavelength-converted signal and conjugate are defined as $k_{4,1}$ and $k_{4,2}$, respectively [13], which are derived as

$$k_{4,1} = \Delta\kappa_{4,1} + \gamma\left(P_S - P_{LO,1}\right) = \beta_2\left[-2\Delta\omega_p^2 - 2\Delta\omega_s\Delta\omega_p\right] + \beta_3\left[-\Delta\omega_p^3 - 2\Delta\omega_s\Delta\omega_p^2 - \Delta\omega_s^2\Delta\omega_p\right] + \gamma\left(P_S - P_{LO,1}\right), \tag{5.1}$$

$$k_{4,2} = \Delta\kappa_{4,2} + \gamma P_{LO,1} = k_{4,1} = \beta_{T,1} - \beta_{T,2} - \beta_{T,3} + \beta_{T,4} + \gamma P_{LO,1} = \beta_2\left[2\Delta\omega_p^2 - 2\Delta\omega_s\Delta\omega_p\right] + \beta_3\left[-\Delta\omega_p^3 + 2\Delta\omega_s\Delta\omega_p^2 - \Delta\omega_s^2\Delta\omega_p\right] + \gamma P_{LO,1}. \tag{5.2}$$

In Eq. (5), $\Delta\kappa_{4,i}$, with i = 1,2, is the phase mismatch due to the material dispersion of the employed fiber; $\beta_{T,v}$, with v = [1,4] is the total dispersion curve of the fiber, which is decomposed using the Taylor series expansion around ω_c (see Fig. 2), where angular frequencies $\omega = 2\pi f$ have been employed in the equations' derivation. β_2 and β_3 are the second and third order dispersion of the fiber, respectively (evaluated at ω_c). The last term of

#242996 Received 15 Jun 2015; revised 14 Aug 2015; accepted 16 Aug 2015; published 21 Aug 2015

$k_{4,i}$ is the phase mismatch due to SPM of the strong reading signal $e_{LO,1}(t)$, being $P_{LO,1}$ its peak power value. The evaluation of Eq. (5) using the values of the previous numerical example leads to $k_{4,1} = 438$ m^{-1} and $k_{4,2} = 2.19\times10^{6}$ m^{-1}, where the dispersion terms β_2 and β_3 has the values $\beta_2 = -4.28\times10^{-2}$ ps^2 and $\beta_3 = 2.39\times10^{-3}$ ps^3.

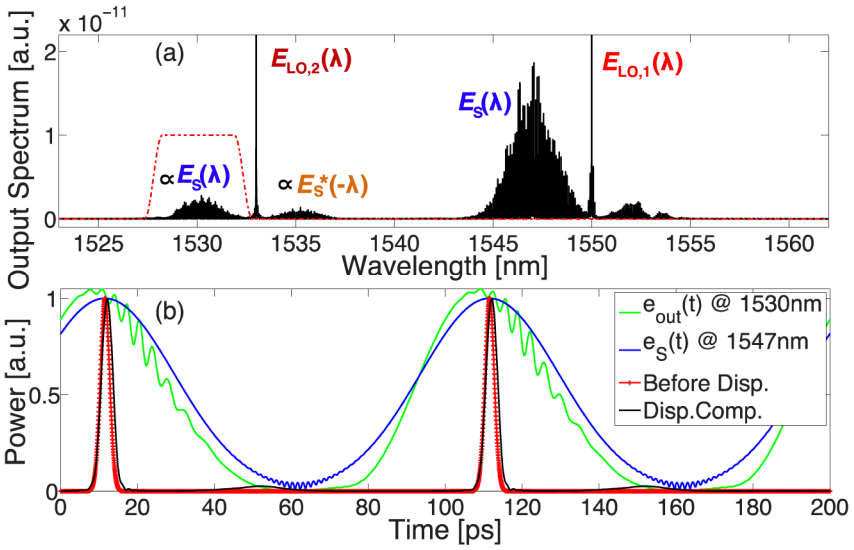

Fig. 3. Results from the numerical simulation of the proposed scheme (no phase-matching) (a) Spectrum at the output of the HNLF; dashed red line represents the applied numerical band-pass filter (BPF). (b) Temporal waveform after the BPF (blue line); transform-limited input before the propagation through the SMF (red line); wavelength-converted output after compensating the dispersion from the SMF (black line).

The high values of $k_{4,1}$ and $k_{4,2}$ clearly indicate that the phase matching condition is not accomplished, suppressing the generation of FWM. In this example, the ZDW has been located at the central wavelength between the probe and the pump. Thus, even with a strong dispersion slope, the group delay values at the wavelengths of probe and pump are nearly identical, reducing the effects of walk-off, which is the main cause of distortion in XPM processes.

Our predictions are confirmed through simulations based on the nonlinear Schrodinger equation, which is numerically solved by the split-step Fourier method [13]. The spectrum at the output of the HNLF is plotted in Fig. 3(a). The spectral component centered at 1530 nm is then filtered in, and the corresponding temporal waveform is shown in Fig. 3(b), together with the original $e_S(t)$. To verify that the output signal has preserved its original phase, we also include in Fig. 3(b) the resulting waveform from propagation through a medium with the exact opposite dispersion to that of a 1-km SMF, and confirm that the dispersion-induced pulse spectral phase has been well compensated for. The difference between the complex envelope of the output signal with respect to the input is attributed to the high S_0, which imposes different group delays to the different frequency components of $e_S(t)$, inducing walk-off in the conversion process.

#242996 Received 15 Jun 2015; revised 14 Aug 2015; accepted 16 Aug 2015; published 21 Aug 2015

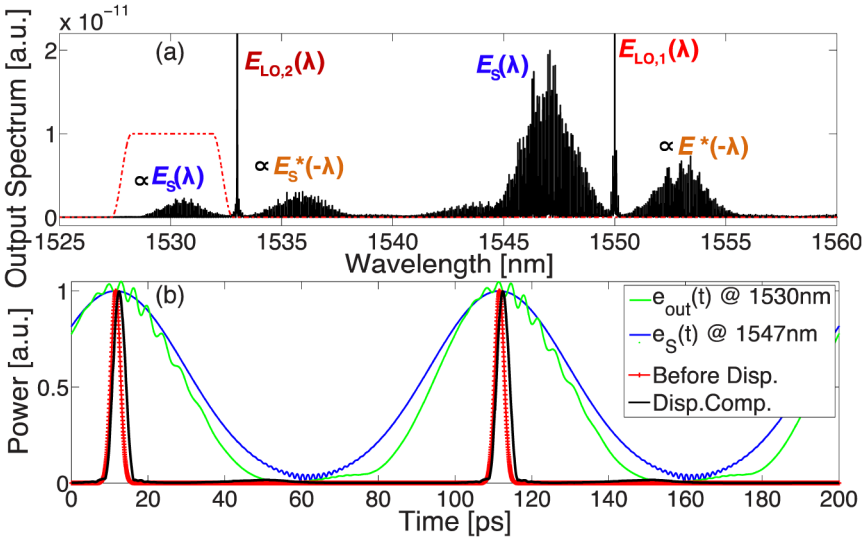

Fig. 4. Results from the numerical simulation of the proposed scheme (a) Spectrum at the output of the HNLF; dashed red line represents the applied numerical band-pass filter (BPF). (b) Temporal waveform after the BPF (blue line); transform-limited input before the propagation through the SMF (red line); wavelength-converted output after compensating the dispersion from the SMF (black line).

In the second example the characteristics of the three signals are the same and in the previous case. The specifications for the HNLF are $\gamma = 11.3\ \mathrm{W^{-1}km^{-1}}$, $L = 1015$ m, the zero dispersion wavelength is 1545 nm and the dispersion slope S_0 (at 1545 nm) = 0.017 ps/nm^2/km. In this case, the solution of Eq. (5) leads to $k_{4,1} = -3.3\times10^{-3}\ \mathrm{m^{-1}}$ and $k_{4,2} = -1.8\times10^{-3}\ \mathrm{m^{-1}}$, for what the first and second order dispersion evaluated at the frequency ω_c results in $\beta_2 = -7.54\times10^{-5}$ ps^2 and $\beta_3 = 2.75\times10^{-5}$ ps^3. These values of phase mismatch suggest that parametric gain due to FWM might still occur in the system. As discussed in Section 2, two idlers proportional to $e_S(t)$ and $e_S^*(t)$ would appear at the frequencies $f_{out,S}$ and $f_{out,-S}$ as a consequence of a mixing between the pumps $e_S(t)$ and $e_{LO,1}(t)$ and the probe signal $e_{LO,2}(t)$. These idlers are proportional to the frequency components generated from XPM around $e_{LO,2}(t)$, and consequently they are added coherently. The obtained spectrum at the output of the HNLF and the resulting temporal output waveform (before and after dispersion compensation) as compared with the input signal are plotted in Fig. 4.

Still, it is worth noticing that in the proposed scheme, only one sufficiently strong CW signal, $e_{LO,1}(t)$, is required as part of the pump, which is additionally undepleted [17], in particular,

$$i_{LO,1} >> |e_{s0}(t)|^2, i_{LO,2} \quad |e_{out}(t)|^2 = 0. \tag{6}$$

This fact suggests that the mixing between the three input signals present at the input of the HNLF would be weak at the output frequencies of interest.

4. Experimental demonstration

In this section, we present an experimental proof-of-concept of the proposed XPM-based wavelength conversion scheme. The experiment setup is shown in Fig. 5. We convert a train of chirped Gaussian-like pulses similar to the one assumed in the above numerical simulations

#242996 Received 15 Jun 2015; revised 14 Aug 2015; accepted 16 Aug 2015; published 21 Aug 2015

(Section 3). The specifications of the employed HNLF are identical to those of the second example presented in Section 3. A configuration with phase matching between signals has been employed due to the limitations imposed by the equipment available in our laboratory.

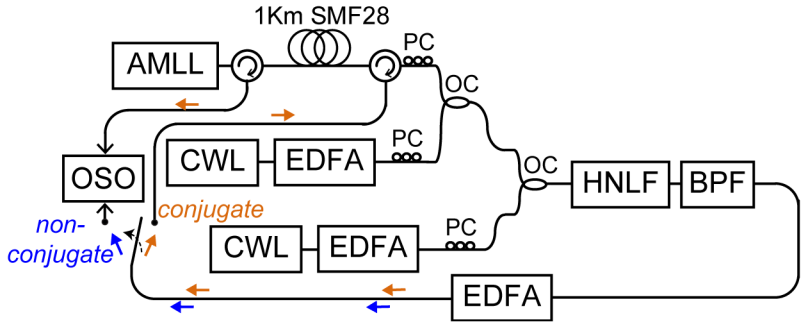

Fig. 5. Experimental setup of the XPM-based wavelength converted scheme for complex signals. AMLL: Active Mode-Locked Laser; PC: Polarization controller; CWL: Continuous-wave laser; EDFA: Erbium-doped fiber amplifier. OSO: Optical sampling oscilloscope.

First, the information signal $e_S(t)$ is generated from a 10-GHz repetition-rate active mode-locked laser (AMLL). The generated pulses have a FWHM of 2.2 ps. To include a quadratic phase to the pulses, the signal propagates through 1 km of SMF, as shown in Fig. 5. The resulting chirped pulses have a FWHM of 27.5 ps. The average power values of the three signals involved in the process, i.e, $e_S(t)$, $e_{LO,1}(t)$ and $e_{LO,2}(t)$ just before the HNLF are coincident with the values provided for the numerical simulation, that is 0.4 dBm, 13 dBm and 3 dBm, respectively. Figure 6 shows the results of the experimental demonstration in three different cases; (a) 17-nm down-conversion of $e_S(t)$, (b) 17-nm up-conversion of $e_S(t)$ and (c) 10-nm down-conversion of $e_S^*(t)$. The first column of Fig. 6 shows the spectrum at the output of the HNLF and the second column shows the corresponding temporal waveforms after filtering in the desired spectral component by a tunable BPF (Santec OTF-350). A 500-GHz optical sampling oscilloscope (Exfo PSO-101) is used to measure the resulting temporal waveforms. The conversion efficiency of the scheme, defined as the ratio of the wavelength converted power at the output facet of the HNLF to the input signal power, varies from −17 dB to −23 dB when the wavelength conversion varies from 7 nm to 17 nm, as shown in Fig. 6. From Fig. 7 we observe that the conversion efficiency for both down-conversion and up-conversion is very similar; this is in sharp contrast to the expected behavior of parametric effects such a FWM, where the down-conversion process is more efficient than the up-conversion due to increased phase mismatch [5]. This suggests that the induced FWM process should be notably weaker than the XPM at the output frequencies, which is consistent with the significant low power of two of the three input signals involved in the mixing process. It is worth it to mention that the obtained conversion efficiency depends on the power of the writing signal, $e_{LO,2}(t)$, as observed from Eq. (4). In this particular proof-of-concept experiment, the power of $e_{LO,2}(t)$ is kept one order of magnitude lower than typical values of pump power in FWM-only based wavelength converters, still achieving similar values of conversion efficiency [3–8]. In all the three reported cases, it is observed that the pulse spectral and temporal shapes of the wavelength-converted signal coincides with those of the original input, proving that the quadratic phase induced by dispersion is preserved. Furthermore, in the case of phase conjugation, Fig. 6(c), we show the waveform of the conjugated signal after propagating again through the 1-km SMF, black line in Fig. 6(c.2), and the results clearly prove that the originally induced dispersion has been well compensated

#242996 Received 15 Jun 2015; revised 14 Aug 2015; accepted 16 Aug 2015; published 21 Aug 2015

for. All experimental results show an excellent agreement with the simulation results in Section 3.

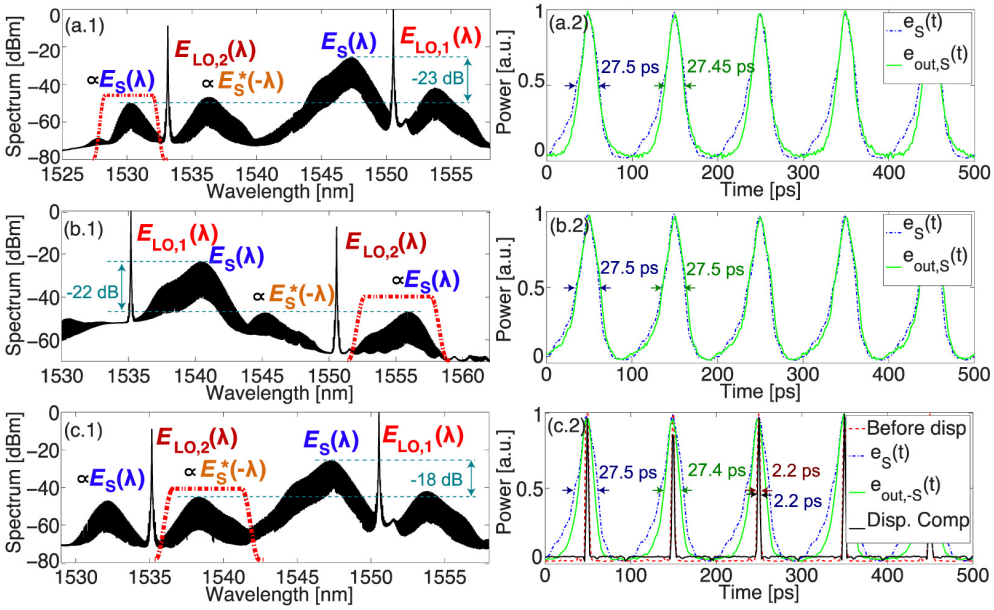

Fig. 6. (a) Down-conversion of $e_S(t)$; (b) Up-conversion of $e_S(t)$; (c) Down-conversion of $e_S^*(t)$; a-c (1) Spectrum after HNLF; a,b (2) Temporal signal after BPF (green line) vs input signal (dashed blue line); c (2) includes output from AMLL (red line) and signal after dispersion compensation (black line).

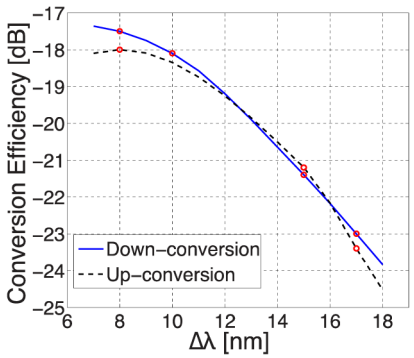

Fig. 7. Conversion efficiency of the XPM-based wavelength converter scheme as a function of the wavelength shift $\Delta\lambda$, for the cases of down-conversion (solid blue line) and up-conversion (dashed black line).

5. Conclusions

A new configuration for wavelength conversion of complex (amplitude and phase) signals based on XPM has been proposed and validated through numerical simulations and experimental demonstration. The proposed scheme uses an all-optical configuration of time-domain holography, and it allows achieving temporal conjugation of the original signal as well. The use of XPM is particularly interesting for wavelength conversion schemes as it enables good conversion efficiency for a broad wavelength range, without the need to accomplish stringent phase matching conditions. Moreover, the obtained conversion efficiency is symmetrical for down- and up-conversion. If the conditions for the occurrence of

#242996 Received 15 Jun 2015; revised 14 Aug 2015; accepted 16 Aug 2015; published 21 Aug 2015

FWM are satisfied, the generated idlers add coherently with the results from XPM, increasing the output power at the frequencies of interest. An additional advantage is that, compared with standard FWM-based implementations, the proposed scheme relaxes the power requirements for the information signal and the output-wavelength CW in more than one order of magnitude for similar conversion efficiency.

#242996 Received 15 Jun 2015; revised 14 Aug 2015; accepted 16 Aug 2015; published 21 Aug 2015